Medical Image Analysis 52 (2019) 119–127

Contents lists available at ScienceDirect

Medical Image Analysis

journal homepage: www.elsevier.com/locate/media

The effect of motion correction interpolation on quantitative *T*1 mapping with MRI

Amitay Nachmani[a,b,1], Roey Schurr[a,1], Leo Joskowicz[a,b], Aviv A. Mezer[a,*]

[a] The Edmond and Lily Safra Center for Brain Sciences, The Hebrew University of Jerusalem, Israel
[b] The Rachel and Selim Benin School of Computer Science and Engineering, The Hebrew University of Jerusalem, Israel

ARTICLE INFO

Article history:
Received 7 April 2018
Revised 29 November 2018
Accepted 30 November 2018
Available online 1 December 2018

Keywords:
Quantitative magnetic resonance imaging
*T*1 map
Motion
Registration
Interpolation and resampling error

ABSTRACT

Quantitative magnetic resonance imaging (qMRI) is a technique for mapping the physical properties of the underlying tissue using several MR images with different contrasts. To overcome subject motion between the acquired images, it is necessary to register the images to a common reference frame. A drawback of registration is the use of interpolation and resampling techniques, which can introduce artifacts into the interpolated data. These artifacts could have unfavorable effects on the accuracy of the estimated tissue's physical properties. Here, we quantified the error of interpolation and resampling on *T*1-weighted images and studied its effects on the mapping of the longitudinal relaxation time (*T*1) using variable flip angles. We simulated *T*1-weighted images and calculated the transformation error resulting from interpolation and resampling. We found that the error is a function of the image contrast (*i.e.*, flip angle) and of the translation and rotation of the image. Furthermore, we found that the error in the *T*1-weighted images has a substantial effect on the *T*1 estimation, of the order of 10% of the signal in the brain's gray and white matter. Hence, minimizing the registration error can enable more accurate *in vivo* modeling of brain microstructure.

1. Introduction

Quantitative magnetic resonance imaging (qMRI) aims to measure the biophysical properties of biological tissue, such as the longitudinal and transverse magnetization relaxation times, *T*1 and *T*2, respectively. Unlike weighted anatomical MR images used in the clinic, qMRI maps aim to remove instrumental biases, yielding interpretable physical units. This measurement of microstructural changes in a tissue non-invasively is considered critical for clinical diagnosis and brain research (Cercignani et al., 2018).

The computation of a qMRI map is based on imaging the same tissue several times, each time varying certain imaging parameters (e.g., time of repetition [TR], time to echo [TE], or flip angle [FA]). The resulting series of images is then used to fit the MR signal equation and extract the unknown biophysical property of interest. Image alignment is a prerequisite for fitting the signal equation: the same coordinate across different images should correspond to the same location in space. *In vivo* scanning of human subjects typically involves some subject motion during the MRI acquisition. To correct for subject motion, the images must be registered to one another. Applying the spatial transformation calculated by the registration process always involves interpolation and resampling of the image (Ashburner and Friston, 2003; Fitzpatrick et al., 2000; Oliveira and Tavares, 2014). This process may insert an error into the transformed image (due to translation and rotation artifacts), which manifests as image blurring. This blurring will increase when neighboring voxel values are very different.

In the registration process, a transformation of the image at hand to a common reference location is calculated assuming an ideal continuous image. To generate the image in the reference location, the image is first interpolated to estimate the continuous image. Next, the image is resampled from the estimated continuous image in the new location. While the resampling process is straightforward, the recovery of the continuous signal using interpolation is not (Aganj et al., 2013; Grevera and Udupa, 1998; Inglada et al., 2006; Kostelec and Periaswamy, 2003; Park and Schowengerdt, 1982; Thévenaz et al., 2000; Tsao, 2003). One of the widely used interpolators for 3D MRI data is the trilinear interpolator. The trilinear interpolator estimates any point of the continuous signal using its closest neighboring voxels, by assuming that the continuous signal changes linearly between neighboring voxels. The estimation of new values from discrete data via interpolation usually introduces some estimation error (Rohde et al., 2009; Tsao, 2003). This error depends on at least three factors. First, the

* Corresponding author.
E-mail address: aviv.mezer@elsc.huji.ac.il (A.A. Mezer).
[1] These authors contributed equally to this work.

https://doi.org/10.1016/j.media.2018.11.012
1361-8415/

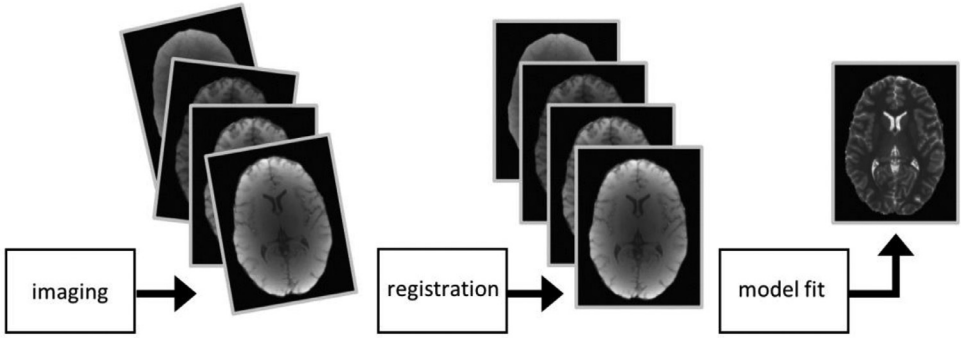

Fig. 1. The process of computing a qMRI $T1$ map. First, the subject is imaged several times with different imaging parameters. Second, the images are registered. Third, a model is fitted to the images to recover the $T1$ map.

distance between measured and sampled coordinate systems (the maximal distance is 0.5 voxel). Second, the difference in measured values between neighboring voxels from which the sampled value is derived (*i.e.*, when all neighboring voxels are similar, the error is minimal). Third, in the case of image rotation, additional error can arise due to aliasing (Oppenheim et al., 1997). The interpolation, resampling and aliasing errors have been discussed and accounted for in many image-processing applications, including MRI (Aganj et al., 2013; Grevera and Udupa, 1998; Huizinga et al., 2016, 2014; Inglada et al., 2006; Kostelec and Periaswamy, 2003; Park and Schowengerdt, 1982; Ramos-Llorden et al., 2017; Thévenaz et al., 2000; Tsao, 2003). The analysis of qMRI poses unique challenges in terms of image registration errors because unlike many other analysis protocols, it is based on multiple images, each with a different contrast.

In this study, we used *in vivo* data to develop a simulation approach for characterizing the potential error introduced into the final qMRI map by the registration process. We focused on a common qMRI protocol used to compute a $T1$ map using multivariate flip-angle acquisitions of spoiled gradient-echo (SPGR) images. In this protocol, $T1$-weighted images with different flip angle are aligned in order to fit the $T1$ (Deoni, 2011; Fram et al., 1987; Mezer et al., 2013; Sereno et al., 2013) (Fig. 1). We quantified the relationship between different flip angles, image contrasts and the magnitude of the interpolation and resampling artifacts due to transformation and rotation. Furthermore, we identified how such artifacts cause errors in the process of $T1$ mapping. Finally, we showed that minimizing this error has a substantial effect on the resulting $T1$ map.

2. Methods

Two simulation analyses were used in this study, as detailed below. One simulates the effects of translation (Fig. 2), and the other simulates the effects of rotation (Fig. 3). The simulated data was based on real *in vivo* $T1$ and $M0$ maps taken from one dataset previously described by Yeatman et al. (2014) (see Section 2.4, Human data acquisition). We used the $T1$ and $M0$ maps of each subject to simulate realistic $T1$-weighted SPGR volumes in the same location as the original maps (ground-truth simulated data), as well as in known locations and orientations in space. Since the spatial transformations between different volumes were known, we were able to apply them using available registration tools. This resulted in a set of motion-corrected $T1$-weighted images (calculated data). By comparing the ground-truth simulated with the motion-corrected calculated data, we could estimate the registration error of each volume. We further fit $T1$ for each set of $T1$-weighted volumes, allowing us to compare the simulated and calculated $T1$ maps. The simulator was coded using MATLAB (The MathWorks Inc., 2015), and the registration of the images was done using the Statistical Parametric Mapping (SPM) toolbox for MATLAB (http://www.fil.ion.ucl.ac.uk/spm/).

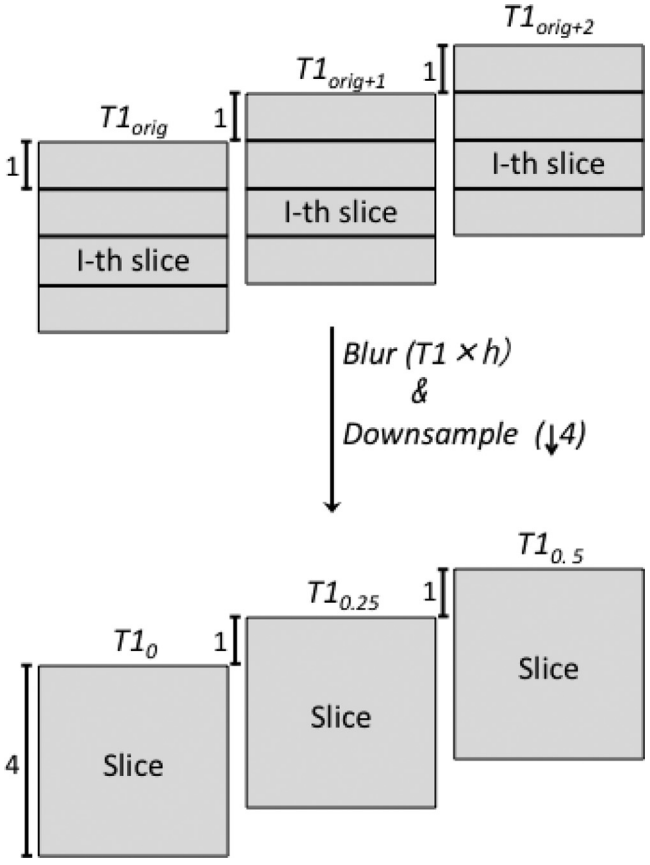

Fig. 2. Simulation of translation. We simulated three identical $T1$ volumes $T1_0$; $T1_{0.25}$; $T1_{0.5}$ in a resolution of $1 \times 1 \times 4$ mm^3. $T1_{0.25}$ and $T1_{0.5}$ volumes are 1 mm and 2 mm away (0.25 and 0.5 of a voxel respectively) from the location of $T1_0$. To simulate the three identical volumes in different locations in space, we first simulated $T1_{orig}$ at $1 \times 1 \times 1$ mm^3 $T1$ map. We then moved $T1_{orig}$ by 1 and 2 mm (1 and 2 voxels respectively) to get $T1_{orig+1}$ and $T1_{orig+2}$ (please note that this full voxel translation does not introduce any change into the image). Next, all the $T1$ maps $T1_{orig}$, $T1_{orig+1}$, and $T1_{orig+2}$ were blurred using full width at half maximum Gaussian kernel (h) and down-sampled by a factor of 4 to get $T1_0$, $T1_{0.25}$ and $T1_{0.5}$, which are a fraction of a voxel away from each other in the new $1 \times 1 \times 4$ mm^3 resolution. Please note that the image illustrates a specific slice, but this was done for all the slices in the volume.

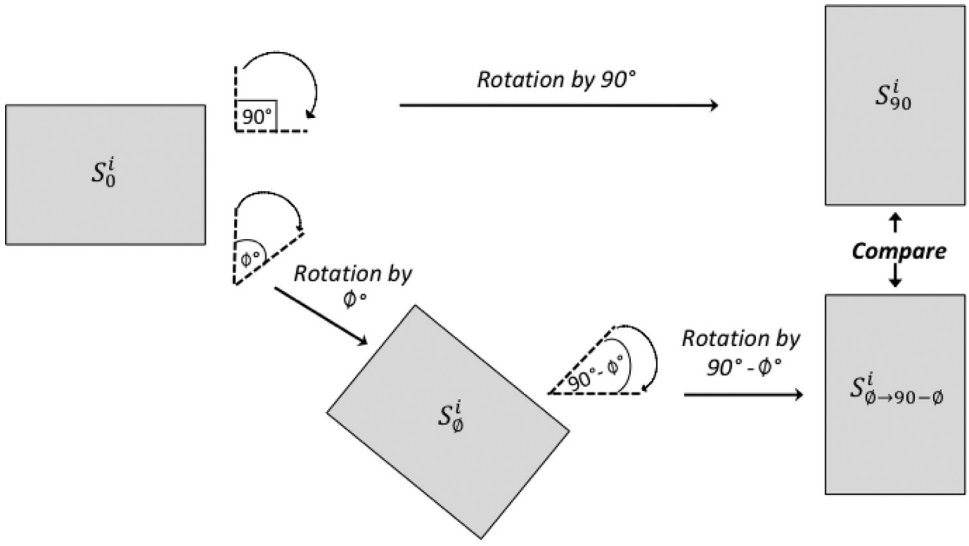

Fig. 3. Simulation of rotation – A $T1$-weighted image $S_{0^\circ}^i$ is rotated by 90° to achieve $S_{90^\circ}^i$. Please note that the 90° rotation keeps the image information identical. Next, the same $S_{0^\circ}^i$ is rotated twice, by $\emptyset^\circ$ and by 90°-$\emptyset^\circ$ to $S_{\phi^\circ\to 90^\circ-\phi^\circ}^i$ that is in the same position as $S_{90^\circ}^i$, yet this image is modified by the rotation process. Lastly, the two images $S_{90^\circ}^i$ and $S_{\phi^\circ\to 90^\circ-\phi^\circ}^i$ can be compared.

2.1. Translation simulations

To study the registration error due to translation and its effect on the final $T1$ map, we simulated for each subject three sets of $T1$-weighted SPGR volumes that were shifted with respect to each other by a fraction of a voxel. These were simulated using each subject's $T1$ and $M0$ maps (see Section 2.4, Human data acquisition), following the two-stage protocol proposed by Greenspan et al. (2002) (Fig. 2).

1. First, we used the subject's $T1$ map to simulate two additional $T1$ volumes that were shifted by 1 or 2 full voxels along the z-direction. Translation by an integer multiple of the sampling step does not introduce any error into the image. Hence, this translation simulates each $T1$ volume as if it were imaged in this new location.
2. Second, to achieve sub-voxel shifts, each volume was blurred using a full width at half maximum Gaussian kernel (h), and down-sampled by a factor of 4 in the z direction (Fig. 2).

This results in three identical volumes that are now a specific fraction of a voxel away from each other in terms of the new, down-sampled voxels ($1\times1\times4$ mm^3): T_0 (non-shifted), $T_{0.25}$ (shifted by 0.25 voxel from T_0) and $T_{0.5}$ (shifted by 0.5 voxel from T_0). A similar procedure was applied to the $M0$ map.

Next, in each location we used the simulated $T1$ and $M0$ maps to simulate $T1$-weighted images with different flip angles (σ), using the SPGR signal equation (Eq. (1)):

$$\mathrm{SPGR}(\sigma) = \frac{M_0\left(1-e^{-TR/T1}\right)\sin\sigma}{\left(1-e^{-TR/T1}\right)\cos\sigma} \tag{1}$$

where TR was based on the *in vivo* scan of each subject. All simulations assumed homogeneous receive-coil and excite-coil fields (B1− and B1+ respectively). We used these three shifted sets of $T1$-weighted images to study the effect of translation on different flip angles, as well as its effect on the final $T1$ map.

To estimate the interpolation and resampling error that is introduced into the $T1$-weighted images of different flip angles, we simulated in each location $T1$-weighted images with flip angles 1–30° (in steps of 1°). We then applied the known spatial transformation to register each volume to the same flip-angle image in the original location (T_0), and calculated the error between the two images (see Section 2.3, Translation and rotation error estimation).

Next, to estimate the error that is introduced into the $T1$ map due to image registration, we compared a simulated $T1$ map in the original location (T_0), using flip angles 4° and 30°, with new $T1$ maps in which one of the flip angles was registered from a shifted set ($T_{0.25}$ or $T_{0.5}$). For example, we used Eq. (1) to fit $T1$ with flip angle 4° in the space of T_0, and flip angle 30° from the space of $T_{0.5}$. Since the spatial transformation between the different sets is known, we did not have to compute the registration (which might introduce further error). Instead, we applied the known spatial transformation to register the shifted data to T_0. This allowed us to compare the ground-truth simulated $T1$ map with the calculated $T1$ map (which is based on registered data).

2.2. Rotation simulations

To calculate the effect of interpolation and resampling due to rotation (Fig. 3), we simulated rotation by different angles. As in the translation simulation above, the rotation was applied on $T1$-weighted images that were simulated using Eq. (1). In contrast to the translation simulations, here the simulated images had a spatial resolution of 1 mm isotropic.

Our protocol followed the work of Owen and Makedon (1996) and included two types of rotations:

Rotation type 1: Volume rotation by 90° away from the origin. Note that for isotropic voxels a 90° rotation does not introduce any error, resulting in $T1$ values identical to those of the simulated volume.

Rotation type 2: Two-step volume rotation: a rotation at an angle of $\emptyset^\circ$, followed by a 90-$\emptyset^\circ$ rotation. The resulting volume has the same final location as the volume that underwent rotation type 1, but it also suffers from interpolation and resampling effects due to the rotations at $< 90^\circ$.

After each rotation step, the rotated image was reconstructed using either trilinear interpolator or a 7th-order b-spline interpolator, both implemented in SPM.

Similar to the translation simulation, the rotated $T1$-weighted images were used to calculate the $T1$ map using Eq. (1). Similar to the translation simulations, we estimated the difference between

the simulated data (rotation type 1) and calculated data (rotation type 2). The difference was calculated both for the rotated *T*1-weighted images at different flip angles and for the fitted *T*1 maps at flip angles 4° and 30°.

2.3. Translation and rotation error estimation

The transformation error (for both translation and rotation simulations) was estimated using the root of the mean squared error (RMSE, Eq. (2)).

Eq. (2) compares images before and after the transformation manipulations (*simulated* and *calculated* respectively). The error was calculated for the difference in each voxel *(v)*, along all the voxels (*N*) within a pre-calculated brain mask. The brain mask was defined using FSL software (Smith et al., 2004; https://fsl.fmrib.ox.ac.uk/), and was further eroded by three voxels in order to avoid edge effects.

We excluded four subjects from the subsequent analysis since their brain mask calculation failed. In addition, we excluded 8 subjects in which errors in the initial *T*1 mapping resulted in extremely high error values (more than three scaled median absolute deviations away from the median across subjects). We further analyzed the remaining 90 subjects.

$$RMSE = \sqrt{\frac{\sum_{v \in N}^{N} \left(calculated(v) - simulated(v)\right)^2}{N}} \quad (2)$$

To compare the RMSE of different *T*1-weighted images (s_i) that were simulated with different flip angles and have different intensities, we z-normalized the images (Eq. (3)).

$$Normalized\ (s_i) = \frac{s_i - Mean\ (s_i)}{STD\ (s_i)} \quad (3)$$

2.4. Human data acquisition

The subjects' data were taken from a larger data set (Yeatman et al., 2014) collected at Stanford University. Data collection procedures were approved by the Stanford University Institutional Review Board. All subjects were healthy and provided informed consent. The data were collected using a 3T General Electric Discovery 750 (General Electric Healthcare, Milwaukee, WI, USA) equipped with a 32-channel head coil (Nova Medical, Wilmington, MA, USA).

The participants were between the ages of 7–85, $N = 102$. For each subject, *T*1 relaxation was measured using several spoiled gradient-echo images (SPGR) acquired at different flip angles (flip angle = 4°, 10°, 20°, 30°); $TR = 14$ ms; $TE = 2.4$ ms, with a spatial resolution of $0.975 \times 0.975 \times 1$ mm^3. The transmit coil inhomogeneity was corrected using a spin-echo inversion-recovery scan (SEIR), using the method presented by Mezer et al. (2016, 2013).

The SEIR scan was scanned with echo-planar imaging read out (EPI), a slab inversion pulse and fat suppression. The imaging parameters for the SEIR-EPI were inversion times = 50, 400, 1200, 2400 ms; $TR = 3$ s; $TE = 47$ ms, and spatial resolution of $2 \times 2 \times 4$ mm^3. The EPI read-out used 2X acceleration to minimize spatial distortions.

The *T*1 fitting procedure results in quantitative *T*1 and *M*0 maps. *T*1 is the measured longitudinal magnetization relaxation time for each voxel in the brain. *M*0 is the maximal initial magnetization in the longitudinal direction.

2.5. Contrast index

*T*1-weighted images with different flip angles have different contrasts. To quantify the contrast of each MRI image, we first segmented the *T*1 map into the three main tissue types (gray matter, white matter and CSF) using k-means that were imitated with the literature's quantitative *T*1 values (Mezer et al., 2016). Next, for each *T*1-weighted image, we calculated the mean value for each tissue type denoted as *Si*, where *i* is the tissue type. The volume's contrast index was defined as the sum of the normalized signal differences between any two tissue types (Eq. (4)).

$$Contrast\ Index = \sum_{i,j\ \in\{WM,\ GM,\ CSF\};i\neq j} \frac{\overline{S_i} - \overline{S_j}}{\overline{(\overline{S_i} + \overline{S_j})/2}} \quad (4)$$

3. Results

In vivo qMRI mapping depends on registration of images with different contrasts to a single location in space. Here, we simulated SPGR *T*1-weighted images in $N = 90$ subjects and tested the effect of interpolation and resampling artifacts on *T*1 mapping. We first show the relation between the contrast of the image and the effect of interpolation and resampling artifacts due to translation (Fig. 4A and B) and rotation (Fig. 4C and D). Next, we show how this contrast-dependent error propagates to the *T*1 mapping, and how minimizing it can improve the fitting accuracy (Fig. 6) and affect the *T*1 effective resolution in space (Fig. 7).

3.1. The effect of contrast on the interpolation error of T1-weighted images

3.1.1. Translation errors

To study the relation between the contrast of the image and the effect of interpolation and resampling artifacts due to translation, we calculated the normalized RMSE of each *T*1-weighted image after it was registered to its original location, and plotted it against the image's flip angle (Fig. 4). We found that the normalized RMSE strongly depends on the flip angle. This dependence is stronger for the maximal possible translation (0.5 voxel shift) compared with smaller translation (0.25 voxel shift; Fig. 4B).

We further tested the effect of interpolation method on the results. We repeated the translation simulations using 7th-order b-spline interpolation. The normalized RMSE were almost identical for the two interpolation methods (mean ± STD for b-spline: 0.0471 ± 0.0163 on average across all subjects and sub-voxel shifts, compared with trilinear interpolation: 0.0469 ± 0.0156; $p < 10^{-10}$, paired-samples *t*-test).

We assumed that the flip angle is related to the error by virtue of its impact on the image contrast (see Eq. (1)). To quantify the contrast dependency on the flip angle, we calculated the contrast index of each image. This contrast index depends on the difference in mean signal between different tissue types (gray matter, white matter and CSF; see Eq. (4)) Fig. 5 shows the agreement between the contrast index and the normalized RMSE in four typical subjects. The value of Pearson's correlation coefficient between the contrast index of the *T*1-weighted images and their normalized RMSE was in the range 0.95–0.99 for all subjects. This high correlation emphasizes the strong dependency between the image contrast and the normalized RMSE following registration. Therefore, images with high contrast seem to be more susceptible to interpolation and resampling artifacts.

3.1.2. Rotation errors

In addition to translation, image registration often involve rotations. Rotation can also introduce interpolation errors, as well as aliasing artifacts. To study the contribution of rotation to the registration error, the simulated *T*1-weighted images were rotated by either 90° (hence introducing no interpolation error) or by two consecutive rotations (∅° and 90-∅°; Fig. 3). Similarly to the case of translation, we found that rotation also introduces greater normalized RMSE for images with higher contrast (Fig. 4C and D).

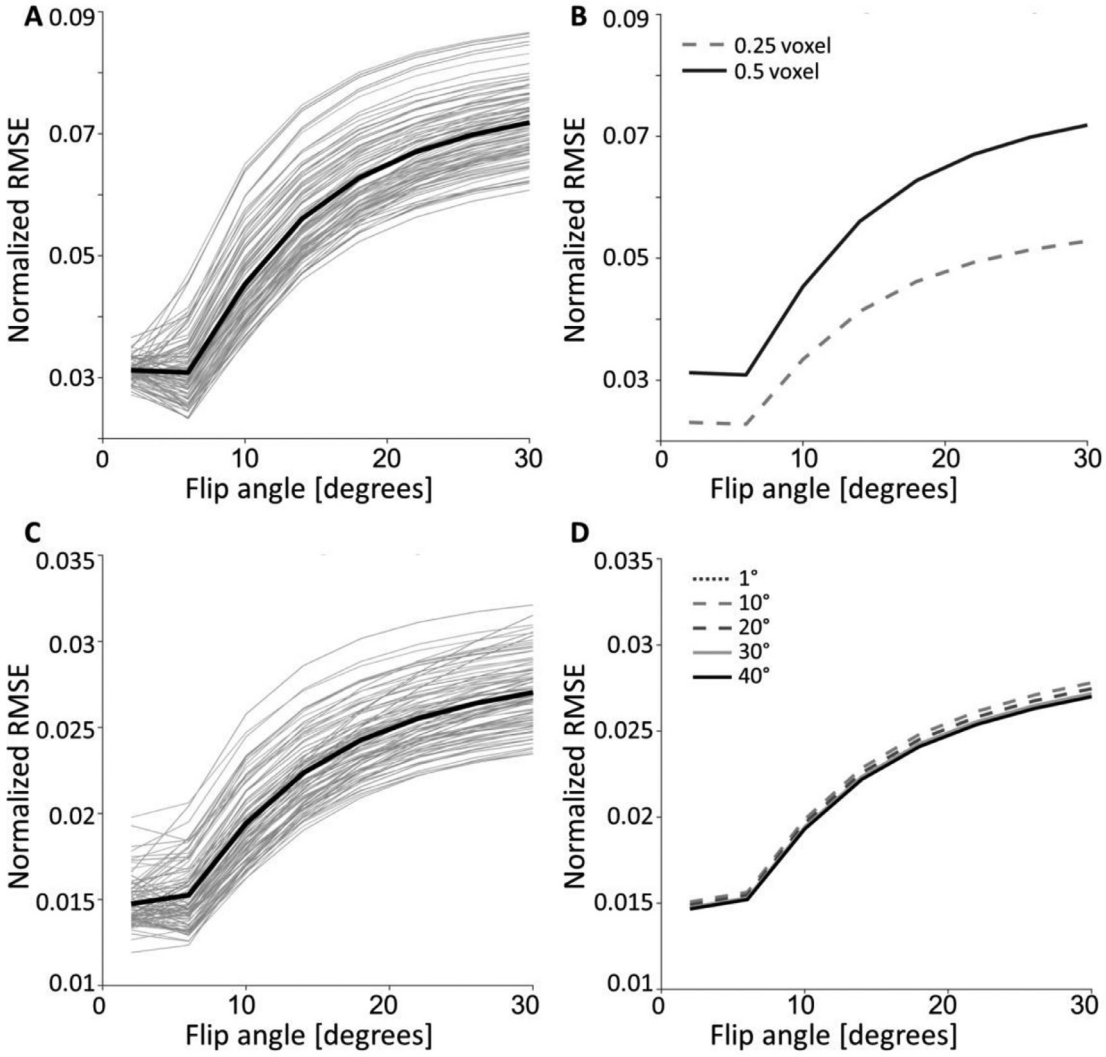

Fig. 4. The error introduced by translation and rotation of *T*1-weighted images as a function flip angle. (A) The normalized root mean square error (RMSE) of 90 subjects (grey lines) after applying the 0.5 voxel translation (see Fig. 2). The RMSE changes as a function of the image's flip angle, which determines the *T*1 weighting of the image (Eq. (1)) and hence its contrast. High contrast images tend to have higher RMSE following translation. Black line shows the mean across subjects. (B) The mean RMSE (across $N = 90$ subject) is greater after applying 0.5 voxel translation (black solid line) compared to applying 0.25 voxel translation (gray dashed line). (C) The RMSE of after applying rotations in 45° (see Fig. 3). Similar to translations, the RMSE change as a function of the image's flip angle. (D) The mean RMSE (across $N = 90$ subjects) is very similar after applying rotations in different angles ($\emptyset = 1°$, 10°, 20°, 30°, 45°). All simulations performed with trilinear interpolation.

We further tested the effect of interpolation method on the results. We repeated the rotation simulations using 7th-order b-spline interpolation. We found lower RMSE values for b-spline interpolation (mean ± STD 0.003 ± 0.001 on average across all subjects and rotation degrees) compared with trilinear interpolation (0.021 ± 0.007; $p < 10^{-100}$, paired-samples *t*-test). The dependence of the *T*1-weighted RMSE on flip angle was similar for both interpolation methods (see Sup. Fig. 1 and Fig. 4C and D).

In theory, the aliasing error is greatest when rotating by 45°. In practice, we found almost no RMSE difference for different rotations ($\emptyset = 1°$, 10°, 20°, 30°, 45°).

This suggests that the main source of error due to rotation is the interpolation, and not aliasing.

Next, we tested how the interpolation of the *T*1-weighted images propagates to the fitted *T*1 map.

3.2. Interpolation effects on T1 mapping

To test how the error in the interpolated *T*1-weighted images propagates into the *T*1 fit, we calculated the RMSE between ground-truth simulated *T*1 maps and the simulated *T*1 maps in which one of the underlying *T*1-weighted images was transformed prior to the fit. Fig. 6 reveals a strong positive relationship between the normalized RMSE of the *T*1-weighted images due to registration and the error in the final *T*1 values that were fitted using these images. This is true for both translation (Fig. 6A; $R^2 = 0.87$) and rotation (Fig. 6B; $R^2 = 0.87$). For translation, the error from maximal translation (0.5 voxel shift) is larger than that from less translation (0.25 voxel shift). For both translation and rotation, a larger error is introduced in the *T*1 map when the transformed *T*1-weighted image has high contrast (flip angle of 30°) compared with low contrast (flip angle of 4°).

A strong relationship between the normalized RMSE of the *T*1-weighted images and the error in *T*1 was also found when we used 7th-order b-spline interpolation (see Sup. Fig. 2 for rotation simulations). The absolute error was smaller for b-spline interpolation. For translation, the error was almost identical for the two interpolation methods (mean + -STD for b-spline: $0.036 + -0.018$ s compared with trilinear interpolation: 0.034 ± 0.017 s; $p < 10^{-84}$, paired-samples *t*-test). For rotation, the effect of interpolation

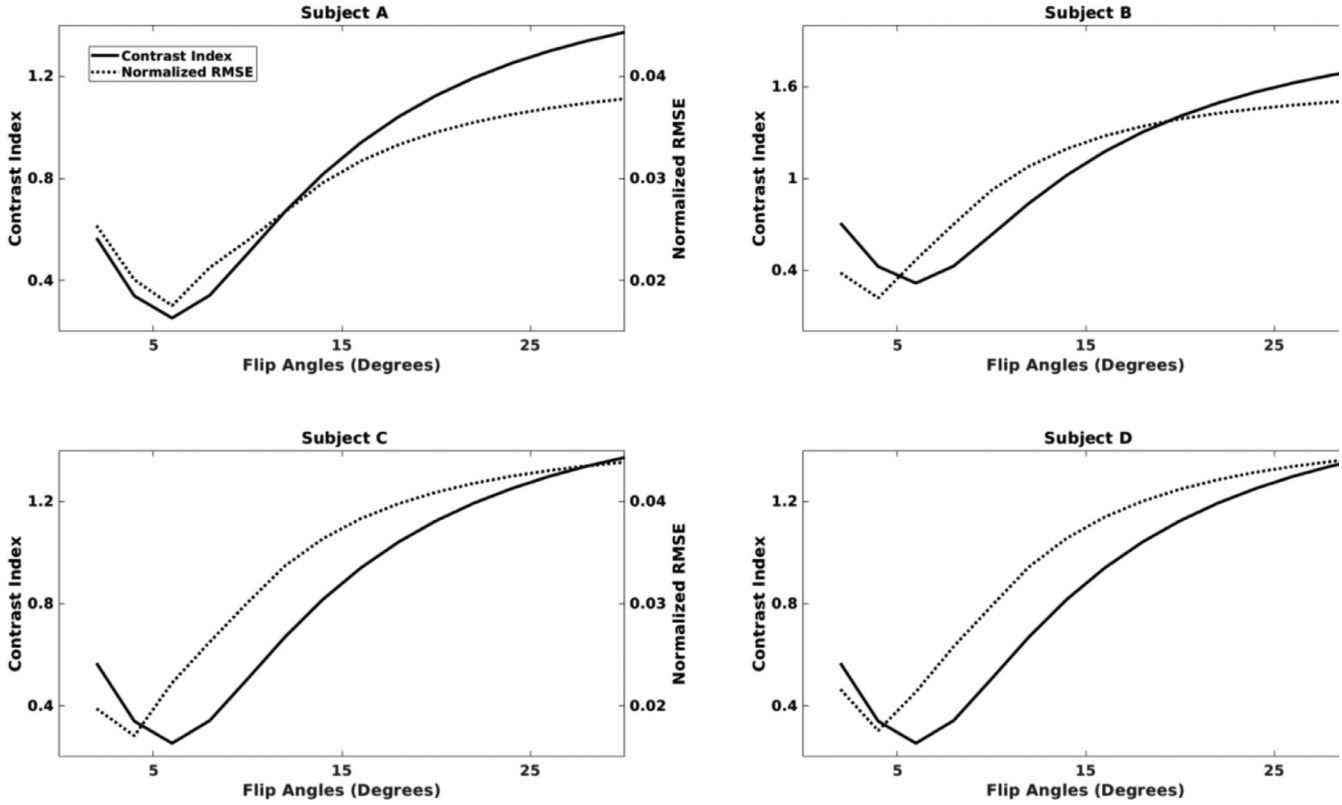

Fig. 5. Registration error vs. image contrast. Four representative subjects' normalized RMSE due to 0.25 voxel translation (solid line, right *y*-axis) and the images' contrast index (dotted line, left y-axis) are plotted for multiple flip angles (*x*-axis). It can be seen that, when the contrast index of the images increases, so does the normalized error introduced following interpolation and resampling. The precision correlation between the two values is very high ($r > 0.95$).

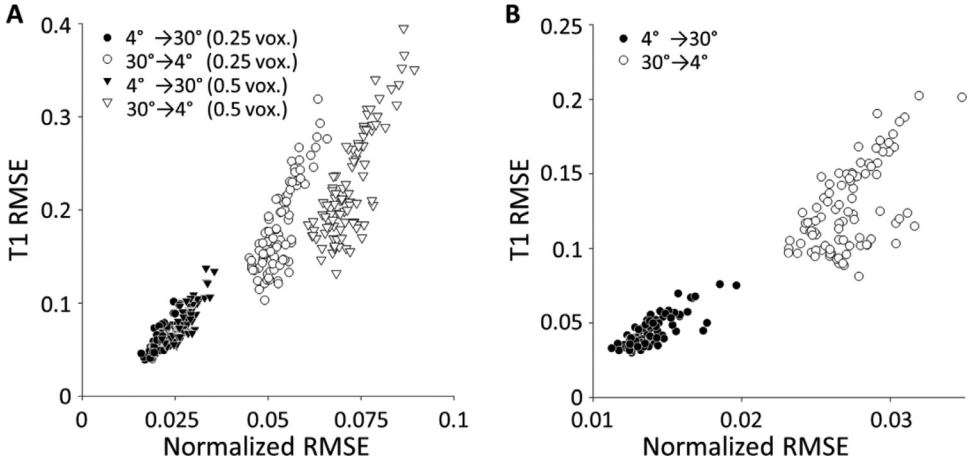

Fig. 6. The error of the *T*1 map is related to the error that is introduces in underlying *T*1-weighted images due to translation and rotation. (A) The normalized root mean squared error (RMSE) in the *T*1 map is strongly related to the error in one of the *T*1-weighted images used for *T*1 fitting ($N = 90$ subjects; $R^2 = 0.87$). The RMSE in the *T*1 map is introduced by registering one of the two *T*1-weighted images to the other. The *T*1-weighted images were simulated for flip angle of 4° (black) or 30° (white), which were simulate with a shift of 0.25 voxels (circles) or 0.5 voxels (triangles). The different *T*1-weighted images have different contrasts, resulting in different errors due to interpolation. (B) A similar relationship is obtained when *T*1-weighted images are rotated by 45° prior to the *T*1 fit ($R^2 = 0.87$). All simulations performed with trilinear interpolation.

method on *T*1 RMSE was greater (RMSE for b-spline interpolation: 0.015 ± 0.007 s, compared with trilinear interpolation: 0.086 ± 0.015 s; $p < 10^{-100}$, paired-samples *t*-test).

To visualize the interpolation and resampling artifacts we compared the *T*1 map with no registration to a map that was generated with registration of either the high-contrast *T*1-weighted image (flip angle of 30°) or a low-contrast *T*1-weighted image (4°) with 0.5 voxel shift (Fig. 7). The interpolation error of the *T*1-weighted images manifests as blurring (filtering of high frequencies) in the *T*1 map. The arrows indicate example regions of *T*1 blurring. In these images, it is clear that the interpolation will affect the identification of borders between different tissue types. We found that the error due to registration is greater when the high-contrast (filp angle 30°) image is interpolated to match the low-contrast (flip angle 4°) image. For images shifted by 0.5 voxel, we found that the *T*1 error is greater by 150 milliseconds on average across subjects when the high-contrast image is registered to the low-contrast image ($p < 10^{-50}$; paired samples *t*-test). This re-

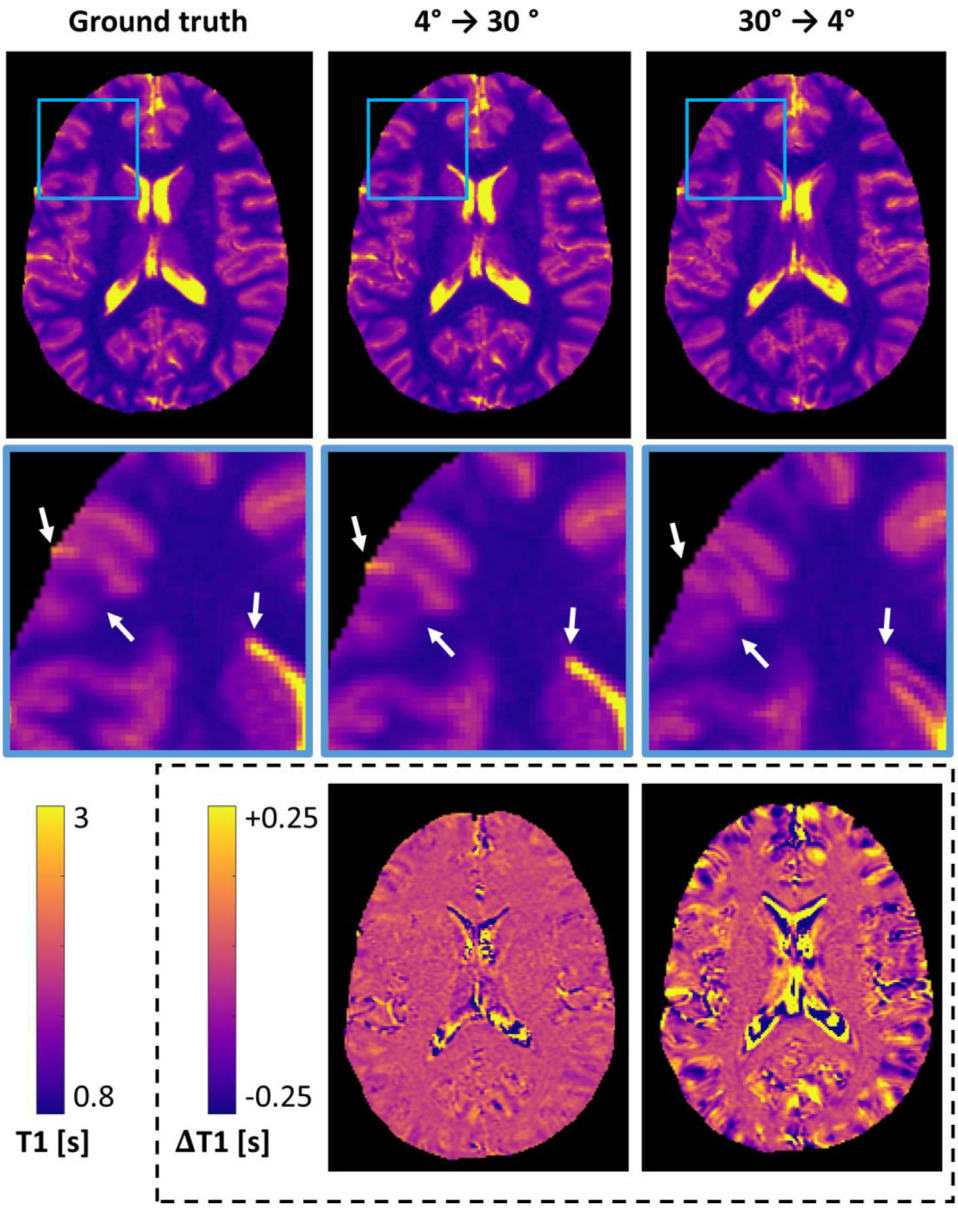

Fig. 7. Interpolation and resampling errors manifest as blurring in the *T*1 map**.** Top: Three *T*1 maps fitted using *T*1-weighted images with flip angles 4° and 30°. *T*1 is calculated either with no translation (left, ground truth *T*1), or with a translation that registers the 4° *T*1-weighted image to the 30° *T*1-weighted image (middle) or the 30° *T*1-weighted image to the 4° *T*1-weighted image (right). Middle row: zoomed-in views of the blue squares. Arrows point to example areas of difference in the spatial information that is maintained due to the registration process. The 4° to 30° registrations better agrees with the original *T*1 map. Box: The difference between the ground-truth *T*1 and the *T*1 map obtained by the appropriate translations of the *T*1-weighted images. Greater error can be seen for registering the high-contrast image to the low-contrast image (right). Errors tend to occur near the border between different tissue types, where the blurring artifacts affect the most.

sult suggests that minimizing the registration interpolation error, by choosing the low-contrast image as the new reference frame, can increase the accuracy of the resulting *T*1 map.

4. Discussion

In vivo MRI is vulnerable to subject motion. For example, intra-scan motion can degrade the quality of the image in both conventional MRI and qMRI. This work focused on motion correction in the context of qMRI techniques. QMRI methods present a special challenge in terms of motion correction as they are also affected by inter-scan motion, *i.e.*, motion between separate acquisitions. Prospective methods have been developed to address inter-scan motion, for example: using navigator echoes (Welch et al., 2004) or optical systems (Aksoy et al., 2011). The current work focused on the effects of retrospective motion correction, in the context of qMRI techniques.

A necessary preprocessing step in fitting a qMRI map involves the registration of several MR images to one common space. This registration requires an estimation of images in a new location in space, and is achieved by interpolation and resampling techniques. Yet interpolation and resampling are imperfect, and lead to the filtering of high frequencies, which manifests itself as blurring of the new image. We found that this blurring effect depends on the exact translation and rotation required for registration. This effect is more severe for images with higher contrast because such images contain more information in high frequencies. When registering MR images with different contrasts to a common new location in space, the question of which location should be chosen arises. We found that, in the case of two images, it is best to move the one

with the lower contrast. We concluded that minimizing the registration interpolation error of the high contrast *T*1-weighted image is beneficial. In the general case of multiple images with different contrast, both the amount of interpolation and image contrast should to be taken into account.

In this work, we studied rigid-body registration, and quantified the error that interpolation and resampling introduce into *T*1-weighted images and into to the resulting fitted *T*1 map. By simulating *T*1-weighted images that are related by known spatial transformations, we were able to disentangle the error that stems from imperfect registration and the error that stems from interpolation and resampling. First, we showed that the interpolation and resampling error stems from the finite approximation of the ideal sinc interpolator (Parker et al., 1983). Then we showed that the interpolation and resampling have the effect of filtering the high frequencies of the estimated image. Furthermore, we showed that this blurring effect is a function of the image contrast and the amount of translation and rotation involved in the registration. Finally, we described how this error propagates to the quantitative *T*1 map, highlighting the need to minimize it. We found that the *T*1 error is ∼150 milliseconds greater when the high-contrast image is interpolated to match the low-contrast image rather than the other way round (for a shift of 0.5 voxels). Notably, this error is comparable to the difference in *T*1 values between different cortical regions, between layers within the cortex, between white-matter sub-regions and between brain regions as a function of age (Benjamini and Basser, 2017; Carey et al., 2017; Marques et al., 2017; Waehnert et al., 2016; Yeatman et al., 2014).

We used a pairwise registration approach in which one image is chosen as a reference image to which all other images are registered. Our findings regarding the differential effects of transforming low-contrast versus high-contrast images are relevant for other registration schemes as well. For example, previous work has suggested using a group-wise registration approach in which all images are considered simultaneously to find an optimal location in space to which all images are registered (Huizinga et al., 2016). Others have unified the motion correction and qMRI parameter fitting into a single optimization problem (Ramos-Llorden et al., 2017). Such approaches could benefit from weighting the different images differently based on their contrast and the amount of translation or rotation applied to them.

Commonly, image registration involves two steps: calculation of the desired spatial transformation, followed by interpolation and resampling of the registered image. It is usually hard to disentangle the errors that result from each of these steps. In this study we followed previous work in using simulated data in which the required spatial transformation is known in advance, both for translation (Greenspan et al., 2002) and rotation (Owen and Makedon, 1996). This allowed us to study the error that stems purely from interpolation and resampling.

The choice of interpolation method had a considerable effect for the resulting RMSE in the rotation simulations, but not in the translation simulations, both for the normalized *T*1-weighted RMSE and for the *T*1-RMSE. Previous work on multiple imaging modalities found a similar trend for the choice of interpolation, although with comparable effects for translation and rotation (Meijering et al., 2001).

In the context of motion correction in quantitative MRI, multiple factors could affect the error in the fitted parameter map (Godenschweger et al., 2016). One such factor is the radiofrequency (RF) transmit field inhomogeneity (B1+). The spatial distribution of B1+ depends on subject position within the scanner, leading to spatially dependent biases in the local flip angle (Boudreau et al., 2017). Estimating B1+ and subject motion separately can therefore lead to incorrect estimations. However, since the B1+ field varies slowly in space, this might not be a concern in the presence of little inter-volume motion. Therefore, in our simulations we used a uniform B1+ field, assuming no spatial inhomogeneity. The receive RF field inhomogeneity (B1−) can also introduce artifacts in the presence of inter-scan subject motion (Papp et al., 2016). Our simulations were designed to isolate and characterize the error that arises from interpolation and resampling, and we therefore assumed a homogeneous receive field.

Recent years have seen great interest in using multiple MR images with variable contrasts to generate quantitative maps that are biophysically meaningful. Such approaches include diffusion imaging, quantitative *T*2, MT and susceptibility mapping (Cercignani et al., 2018). While we tested the effect of interpolation and resampling error due to registration on quantitative *T*1, it is reasonable to assume that a similar error will be introduced into any other quantitative approach that uses different images with very different contrasts. Recently, several approaches were proposed to minimize this registration error for qMRI (Huizinga et al., 2016; Papp et al., 2016; Ramos-Llorden et al., 2017). The results of this study highlight the importance of taking these issues into consideration when mapping quantitative MRI parameters, and the need for developing new methods specially tailored for qMRI.

Funding

This work was supported by the joint funding program between the National Science United States-Israel Binational Science Foundation (BCS1551330 to AAM and Jason D. Yeatman); The Israel Science Foundation (0399306 to AAM) and a seed grant from the Eric Roland Fund for Interdisciplinary Research administered by ELSC, awarded to AAM and RS.

Declarations of interest:

None.

Acknowledgments

The authors thank Shai Berman and Jonathan S. Bain for their constructive comments and suggestions.

Supplementary material

Supplementary material associated with this article can be found, in the online version, at doi:10.1016/j.media.2018.11.012.

References

Aganj, I., Yeo, B.T.T., Sabuncu, M.R., Fischl, B., 2013. On removing interpolation and resampling artifacts in rigid image registration. IEEE Trans. Image Process. 22, 816–827.

Aksoy, M., Forman, C., Straka, M., Skare, S., Holdsworth, S., Hornegger, J., Bammer, R., 2011. Real-time optical motion correction for diffusion tensor imaging. Magn. Reson. Med. 66, 366–378. https://doi.org/10.1002/mrm.22787.

Ashburner, J., Friston, K., 2003. Rigid body registration. In: Human Brain Function: Second Edition, pp. 635–653.

Benjamini, D., Basser, P.J., 2017. Magnetic resonance microdynamic imaging reveals distinct tissue microenvironments. Neuroimage 163, 183–196.

Boudreau, M., Tardif, C.L., Stikov, N., Sled, J.G., Lee, W., Pike, G.B., 2017. B1 mapping for bias-correction in quantitative T1 imaging of the brain at 3T using standard pulse sequences. JMRI 1–10. https://doi.org/10.1002/jmri.25692.

Carey, D., Caprini, F., Allen, M., Lutti, A., Weiskopf, N., Rees, G., Callaghan, M.F., Dick, F., 2017. Quantitative MRI provides markers of intra-, inter-regional, and age-related differences in young adult cortical microstructure. Neuroimage..

Cercignani, M., Dowell, N.G., Tofts, P.S., 2018. Quantitative MRI of the Brain: Principles of Physical Measurement, second ed. Taylor & Francis.

Deoni, S.C.L., 2011. Magnetic resonance relaxation and quantitative measurement in the brain. In: Magnetic Resonance Neuroimaging, pp. 65–108.

Fitzpatrick, J.M., Hill, D.L.G., Maurer, C.R., 2000. Image registration. In: Handbook of Medical Imaging, Volume 2: Medical Image Processing and Analysis, pp. 447–513.

Fram, E.K., Herfkens, R.J., Johnson, G.A., Glover, G.H., Karis, J.P., Shimakawa, A., Perkins, T.G., Pelc, N.J., 1987. Rapid calculation of T1 using variable flip angle gradient refocused imaging. Magn. Reson. Imaging 5, 201–208.

Greenspan, H., Oz, G., Kiryati, N., Peled, S., 2002. MRI inter-slice reconstruction using super-resolution. Magn. Reson. Imaging 20, 437–446.
Godenschweger, F., Kägebein, U., Stucht, D., Yarach, U., Sciarra, A., Yakupov, R., Lüsebrink, F., Schulze, P., Speck, O., 2016. Motion correction in MRI of the brain. Phys. Med. Biol. 61, R32–R56. https://doi.org/10.1088/0031-9155/61/5/R32.
Grevera, G.J., Udupa, J.K., 1998. An objective comparison of 3-D image interpolation methods. IEEE Trans. Med. Imaging 17, 642–652.
Huizinga, W., Poot, D.H.J., Guyader, J.-M., Klaassen, R., Coolen, B.F., van Kranenburg, M., van Geuns, R.J.M., Uitterdijk, A., Polfliet, M., Vandemeulebroucke, J., Leemans, A., Niessen, W.J., Klein, S., 2016. PCA-based groupwise image registration for quantitative MRI. Med. Image Anal. 29, 65–78.
Huizinga, W., Poot, D.H.J., Guyader, J.-M., Smit, H., van Kranenburg, M., van Geuns, R.-J.M., Uitterdijk, A., van Beusekom, H.M.M., Coolen, B.F., Leemans, A., Niessen, W.J., Klein, S., 2014. Non-rigid Groupwise Image Registration for Motion Compensation in Quantitative MRI. Springer, Cham, pp. 184–193.
Inglada, J., Muron, V., Pichard, D., Feuvrier, T., 2006. Analysis of artifacts in sub-pixel remote sensing image registration. In: Revue Francaise de Photogrammetrie et de Teledetection, pp. 29–34.
Kostelec, P.J., Periaswamy, S., 2003. Image registration for MRI. Mod. Signal Process. 46, 161–184.
Marques, J.P., Khabipova, D., Gruetter, R., 2017. Studying cyto and myeloarchitecture of the human cortex at ultra-high field with quantitative imaging: R 1, R 2 * and magnetic susceptibility. Neuroimage 147, 152–163.
Meijering, E.H.W., Niessen, W.J., Viergever, M.A., 2001. Quantitative evaluation of convolution-based methods for medical image interpolation. Med. Image Anal. 5, 111–126. https://doi.org/10.1016/S1361-8415(00)00040-2.
Mezer, A., Rokem, A., Berman, S., Hastie, T., Wandell, B.A., 2016. Evaluating quantitative proton-density-mapping methods. Hum. Brain Mapp 37, 3623–3635.
Mezer, A., Yeatman, J.D., Stikov, N., Kay, K.N., Cho, N.-J., Dougherty, R.F., Perry, M.L., Parvizi, J., Hua, L.H., Butts-Pauly, K., Wandell, B.A., 2013. Quantifying the local tissue volume and composition in individual brains with magnetic resonance imaging. Nat. Med. 19, 1667–1672.
Oliveira, F.P.M., Tavares, J.M.R.S., 2014. Medical image registration: a review. Comput. Methods Biomech. Biomed. Eng. 17, 73–93.
Oppenheim, A.V, Willsky, A.S., Nawab, S.H., 1997. Signals and Systems.
Owen, C.B., Makedon, F., 1996. High quality alias free image rotation. In: Conf. Rec. Thirtieth Asilomar Conf. Signals, Syst. Comput., 1, pp. 2–6.
Papp, D., Callaghan, M.F., Meyer, H., Buckley, C., Weiskopf, N., 2016. Correction of inter-scan motion artifacts in quantitative R1 mapping by accounting for receive coil sensitivity effects. Magn. Reson. Med. 76, 1478–1485.
Park, S.K., Schowengerdt, R.a, 1982. Image sampling, reconstruction, and the effect of sample-scene phasing. Appl. Opt. 21, 3142–3151.
Parker, J.A., Kenyon, R.V., Troxel, D.E., 1983. Comparison of interpolating methods for image resampling. IEEE Trans. Med. Imaging 2, 31–39.
Ramos-Llorden, G., den Dekker, A.J., Van Steenkiste, G., Jeurissen, B., Vanhevel, F., Van Audekerke, J., Verhoye, M., Sijbers, J., 2017. A unified maximum likelihood framework for simultaneous motion and T1 estimation in quantitative MR T1 mapping. IEEE Trans. Med. Imaging 36, 433–446.
Rohde, G.K., Aldroubi, A., Healy, D.M., 2009. Interpolation artifacts in sub-pixel image registration. IEEE Trans. Image Process. 18, 333–345.
Smith, S.M., Jenkinson, M., Woolrich, M.W., Beckmann, C.F., Behrens, T.E.J., Johansen-Berg, H., Bannister, P.R., De Luca, M., Drobnjak, I., Flitney, D.E., Niazy, R., Saunders, J., Vickers, J., Zhang, Y., De Stefano, N., Brady, J.M., M., P.M., 2004. Advances in functional and structural MR image analysis and implementation as FSL. Neuroimage 23, 208–219.
Sereno, M.I., Lutti, A., Weiskopf, N., Dick, F., 2013. Mapping the human cortical surface by combining quantitative T1 with retinotopy. Cereb. Cortex 23, 2261–2268.
The MathWorks Inc., 2015. MATLAB Version R2015b, Massachusetts, U.S.A.
Thévenaz, P., Blu, T., Unser, M., 2000. Interpolation revisited. IEEE Trans. Med. Imaging 19, 739–758.
Tsao, J., 2003. Interpolation artifacts in multimodality image registration based on maximization of mutual information. IEEE Trans. Med. Imaging 22, 854–864.
Waehnert, M.D., Dinse, J., Schäfer, A., Geyer, S., Bazin, P.-L., Turner, R., Tardif, C.L., 2016. A subject-specific framework for *in vivo* myeloarchitectonic analysis using high resolution quantitative MRI. Neuroimage 125, 94–107.
Welch, E.B., Manduca, A., Grimm, R.C., Jack, C.R., 2004. Interscan registration using navigator echoes. Magn. Reson. Med. 52, 1448–1452. https://doi.org/10.1002/mrm.20275.
Yeatman, J.D., Wandell, B.A., Mezer, A.A., 2014. Lifespan maturation and degeneration of human brain white matter. Nat. Commun. 5, 4932.